

Local structure of calcium silicate melts from classical molecular dynamics simulation and a newly constructed thermodynamic model

Yong-quan WU, Chen DAI, Guo-chang JIANG

Shanghai Key Laboratory of Modern Metallurgy & Materials Processing,
School of Materials Science and Engineering, Shanghai University, Shanghai 200072, China

Received 14 June 2013; accepted 18 December 2013

Abstract: The distributions of local structural units of calcium silicate melts were quantified by means of classical molecular dynamics simulation and a newly constructed structural thermodynamic model. The distribution of five kinds of Si–O tetrahedra Q_i from these two methods was compared with each other and also with the experimental Raman spectra, an excellent agreement was achieved. These not only displayed the panorama distribution of microstructural units in the whole composition range, but also proved that the thermodynamic model is suitable for the utilization as the subsequent application model of spectral experiments for the thermodynamic calculation. Meanwhile, the five refined regions mastered by different disproportionating reactions were obtained. Finally, the distributions of two kinds of connections between Q_i were obtained, denoted as Q_i –Ca– Q_j and Q_i –[O_b]– Q_j , from the thermodynamic model, and a theoretical verification was given that the dominant connections for any composition are equivalent connections.

Key words: distribution of microstructural units; molecular dynamic simulation; structural thermodynamic model; calcium silicate melts

1 Introduction

Properties of calcium silicate melts, such as viscosity, configurational entropy, are directly related to their microstructure, especially the distribution of Si–O tetrahedra and their connections. Investigations on the microstructure of calcium silicate melts, therefore, are fundamental towards understanding the physical properties of metallurgical slag [1], geological magmas [2], and ceramic materials [3], which control the mechanism of practical phenomena. The vital of all to master the physicochemical behavior of calcium silicate melts is the measurement of the relative abundances of microstructural units and their mixing properties from computational [4–8] and spectral experiments [9–12], as well as some theoretical models [13,14].

Up to now, most studies were concentrated on the silicate glasses instead of melts because of the harsh experimental condition of high liquidus temperature up to 1700–2000 K for silicate melts. In 1970, SHUKER

and GAMMON [15] presented the outline of a calculation leading to an equation for the spectral scattering intensity (especially the Raman intensity) in terms of the density of states of the vibrations in amorphous materials. Since then, hundreds of works were reported on the study of the scattering coefficients, but all of them were concentrated on the low-frequency region, where the boson peak is located in. Therefore, the quantification of microstructural units from deconvolution of envelope is still far from resolution. So far, the investigations of silicate glasses under atmospheric pressure identified the basic structural units as five kinds of Si–O tetrahedrons, denoted as Q_i , where i represents the number of bridging oxygen, with the utilization of Raman spectroscopy [15–18] and ^{29}Si NMR [19,20]. Besides, in order to move away the stone of high temperature, the new technique of high-temperature Raman spectroscopy [21] has also been developed in the past decade. Recently, our newly theoretical research [22] has also partly resolved the evaluation of Raman coupling coefficient and its

Foundation item: Project (2012CB722805) supported by the National Basic Research Program of China; Projects (50504010, 50974083, 51174131, 51374141) supported by the National Natural Science Foundation of China; Project (50774112) supported by the Joint Fund of NSFC and Baosteel, China; Project (07QA4021) supported by the Shanghai “Phosphor” Science Foundation, China

Corresponding author: Yong-quan WU; Tel: +86-21-56332144; E-mail: yqw@shu.edu.cn

DOI: 10.1016/S1003-6326(14)63217-9

Integration-Raman scattering coefficient. Thus, the quantification of Raman spectra can be achieved. On the other hand, the obstacle of high temperature means nothing for “computer experiments”, such as molecular dynamic simulation and Monte Carlo method. Even so, all knowledge about the microstructure from Raman spectral measurement and “computer experiments” is still discrete. To obtain the panorama of distribution of microstructural units, a structural thermodynamic model is indispensable.

In this work, two kinds of results about the unique distribution of tetrahedral units for calcium silicate melts from classic molecular dynamics simulation, and a structural thermodynamic model, as well as the in-situ high-temperature Raman spectral (HTRS) measurement are presented and compared with each other. One of ultimate functions of this work is to serve as the basis and complete knowledge about microstructural distributions for some structural or formulated models applied for the calculations of spectral, thermodynamic and transporting properties.

2 Description of theoretical calculation and experimental measurement

2.1 Molecular dynamics simulation

The MD simulation code applied in this study is MOLLY version 2.26 from Department of Earth Sciences, UK, with the insertion of our own designed analysis module of equilibrium configurations. All ions in the simulation are treated as rigid with their formal charges: Ca^{2+} , Si^{4+} , and O^{2-} . The potential applied in these simulations is of two-body Born–Mayer–Huggins (BMH) form that has been tested in the previous work [22]:

$$u(r_{ij}) = q_i q_j e^2 / r_{ij} + f_0 B_{ij} \exp[(\sigma_i + \sigma_j - r_{ij}) / \rho_{ij}] \quad (1)$$

where $u(r_{ij})$ is the interatomic potential and r_{ij} denotes the interatomic distance. The first term in the right side represents Coulomb interaction and the second term is inter-core short-range repulsion. For three pairs of Si–Si, Si–O and O–O, the values sourced from OKADA et al [23], in which the two parameters of B_{ij} , and ρ_{ij} expressed as $B_{ij} = \rho_{ij} = b_i + b_j$, are used; for the rest three pairs applied are the values from KIEFFER and ANGELL [24], in which the parameter of B_{ij} is expressed as $B_{ij} = 1 + q_i / n_i + q_j / n_j$ where n_i represents the number of out-shell electrons in atom i , and ρ_{ij} is maintained constant, 0.029 nm. Because of the different expressions between OKADA et al [23] and KIEFFER and ANGELL [24] for B_{ij} , the parameter of f_0 has different physical meanings and units just as listed in Table 1.

The canonical ensemble employing Nosé–Hoover thermostat [25] for the temperature control is used for the

Table 1 Parameters for Born–Mayer–Huggins (BMH) potential

Source	Pair	i	σ_i/nm	n_i or b_i/nm	f_0
a	Si–Si	Si	0.064	0.00125	6.9472×10^{-11} N
	Si–O				
	O–O	O	0.184	0.013	
b	Ca–Si	Si	0.131	7	1.916043×10^{-20} J
	Ca–O	O	0.142	10	
	Ca–Ca	Ca	0.158	8	

^a from OKADA et al [23]; ^b from KIEFFER and ANGELL [24].

structural relaxation runs. In this work, the initial configuration is generated with “skew start” method [26], which is proven to be very fitting for the simulation of liquid state. The initial velocities of ions are chosen from the Maxwell–Boltzmann distribution [27] at the specified initial temperature of 6000 K. After the structural relaxation of about 3000 steps, the objective temperature of 2000 K is reset. Another 5000 steps are used to achieve the systematic equilibrium. Then, the relative abundance of tetrahedral units is averaged for 5000 equilibrium configurations obtained every other 120 steps with a defined cutoff Si–O distance of 0.2 nm, which corresponds to the position of the first minimum of Si–O partial radial distribution function (RDF). So, the total number of simulation steps is 608000. Because the time step is set as 0.001 ps, the total simulating time is 608 ps. Finally, the compositions and ionic number of all samples in MD simulation are listed in Table 2.

Table 2 Molar fraction and ionic number of samples in MD simulation

Sample	Molar fraction of CaO	Ionic number			
		Ca	Si	O	Total
C30S70	0.30	111	259	629	999
C35S65	0.35	132	245	622	999
C40S60	0.40	154	231	616	1001
C45S55	0.45	176	216	608	1000
C50S50	0.50	200	200	600	1000
C55S45	0.55	224	184	592	1000

2.2 Structural thermodynamics of self-consistent model

This structural thermodynamic model treats the calcium silicate melts with seven structural units: dissociative Ca^{2+} , free oxygen O^{2-} and five kinds of Si–O tetrahedral units denoted as Q_i . Therefore, for one system, two sets of components will be used in the deduction of this model: one is the macro components of $\{X_{\text{CaO}}, X_{\text{SiO}_2}\}$, the other is the micro structural units of $\{X_{\text{Ca}}, X_{\text{O}}, X_{\text{Q}_0}, X_{\text{Q}_1}, X_{\text{Q}_2}, X_{\text{Q}_3}, X_{\text{Q}_4}\}$, where X_i represents the molar fraction of component or unit i . It is obvious that these two sets of components have some correlations

with each other, in which only two correlations are independent and we can write them as

$$\sum_{i=0}^4 X_{Q_i} / \left(\sum_{i=0}^4 X_{Q_i} + X_{Ca} \right) = X_{SiO_2} \quad (2)$$

$$\left(\sum_{i=0}^4 \left(4 - \frac{i}{2} \right) X_{Q_i} + X_O \right) / \sum_{i=0}^4 X_{Q_i} = 2 + X_{CaO} / X_{SiO_2} \quad (3)$$

As we know, Gibbs free energy of a system is contributed by enthalpy and entropy, where the entropy can be further divided into two parts of the configuration and non-configuration.

$$G = H - TS = H - T \left(S^{cf} + S^{ncf} \right) = \sum_{i=0}^4 H_{Q_i} - T \left(S^{cf} + \sum_{i=0}^4 S_{Q_i}^{ncf} \right) \quad (4)$$

where the enthalpy and non-configurational entropy are treated as the sum of characteristic enthalpies and entropies of five tetrahedral units because Ca^{2+} and O^{2-} are both single atomic units. Then the Gibbs free energy can be rewritten as

$$G = \sum_{i=0}^4 X_{Q_i} H_{Q_{i,0}} - T \left(S^{cf} + \sum_{i=0}^4 X_{Q_i} S_{Q_{i,0}}^{ncf} \right) = \sum_{i=0}^4 X_{Q_i} H_{Q_{i,0}} - T \sum_{i=0}^4 X_{Q_i} S_{Q_{i,0}}^{ncf} - TS^{cf} = G^\circ - TS^{cf} \quad (5)$$

where the subscript 0 represents the molar quantities, namely $H_{Q_{2,0}}$ and $S_{Q_{2,0}}^{ncf}$ represent the characteristic enthalpy and entropy per mole of unit Q_2 . The term of G° represents the free energy of independent system of Q_i , in which each Q_i has no interactions with others.

$$G^\circ = \sum_{i=0}^4 X_{Q_i} H_{Q_{i,0}} - T \sum_{i=0}^4 X_{Q_i} S_{Q_{i,0}}^{ncf} \quad (6)$$

Thus, the 10 parameters of characteristic enthalpies $H_{Q_{i,0}}$ and non-configurational entropies $S_{Q_{i,0}}^{ncf}$ are the inner properties of Q_i and can be directly calculated from the spectral or calorimetric enthalpies and entropies of corresponding single crystals. For instance, the single crystal $CaSiO_3$ has only one kind of tetrahedral unit Q_2 , so its enthalpy and entropy can be defined as the characteristic enthalpy and entropy of Q_2 , respectively. In addition to the contribution of configurational entropy, which represents the connections between Q_i s, we can make the independent system into the real melt, interacting system.

For the configurational entropy is directly related with the spatial topology of the seven microstructural units, two contributions should be considered, one is the connection between tetrahedral units via Q_i-Ca-Q_j and the other is that via $Q_i-[O_b]-Q_j$, where O_b is the bridging

oxygen and the brackets indicate that O_b is co-possessed by two tetrahedra. The molar fraction of X_i is corresponding to the number of structural units of n_i . By extending the thought of quasi-lattice model of YOKOKAWA and NIWA [14], all the structural units should be arranged into the lattice points. Firstly, the connection centers of Ca and O_b should be distributed and the number of ways of distribution of these two kinds of centers is given by

$$\left(\sum_{i=1}^4 in_{Q_i} / 2 + n_{Ca} \right) ! / \left(n_{Ca} ! \left(\sum_{i=1}^4 in_{Q_i} / 2 \right) ! \right).$$

The distributions of two kinds of connections are listed in Table 3.

Table 3 Distribution of two kinds of connections

Q_i-Ca-Q_j		$Q_i-[O_b]-Q_j$	
Connection	Total number of connection	Connection	Total number of connection
Q_0-Ca-Q_0	r_{00}	$Q_1-[O_b]-Q_1$	b_{11}
Q_0-Ca-Q_1	r_{01}	$Q_1-[O_b]-Q_2$	b_{12}
Q_0-Ca-Q_2	r_{02}	$Q_1-[O_b]-Q_3$	b_{13}
Q_0-Ca-Q_3	r_{03}	$Q_1-[O_b]-Q_4$	b_{14}
Q_1-Ca-Q_1	r_{11}	$Q_2-[O_b]-Q_2$	b_{22}
Q_1-Ca-Q_2	r_{12}	$Q_2-[O_b]-Q_3$	b_{23}
Q_1-Ca-Q_3	r_{13}	$Q_2-[O_b]-Q_4$	b_{24}
Q_2-Ca-Q_2	r_{22}	$Q_3-[O_b]-Q_3$	b_{33}
Q_2-Ca-Q_3	r_{23}	$Q_3-[O_b]-Q_4$	b_{34}
Q_3-Ca-Q_3	r_{33}	$Q_4-[O_b]-Q_4$	b_{44}
Total	$n_{Ca}-n_O$	Total	$\sum_{i=1}^4 in_{Q_i} / 2$

Obviously, Q_4 does not appear in the first connection because it has no non-bridging oxygen, O_{nb} . Similarly, the second connection has no Q_0 because Q_0 has no bridging oxygen, O_b . Then, the numbers of ways of these two kinds of distributions are given by

$$(n_{Ca} - n_O) ! / \left(\left(\prod_{i=0}^3 r_{ii} ! \right) \prod_{i=0}^3 \prod_{j=i+1}^3 \left(\frac{r_{ij}}{2} ! \frac{r_{ij}}{2} ! \right) \right)$$

where r_{ij} represents the number of Q_i-Ca-Q_j and

$$\left(\sum_{i=1}^4 in_{Q_i} / 2 \right) ! / \left(\left(\prod_{i=1}^4 b_{ii} ! \right) \prod_{i=1}^4 \prod_{j=i+1}^4 \left(\frac{b_{ij}}{2} ! \frac{b_{ij}}{2} ! \right) \right)$$

where b_{ij} is the number of $Q_i-[O_b]-Q_j$. It should be noted that the free oxygen is also distributed. Because free oxygen always coordinates with calcium, the number of ways of this distribution is given by $n_{Ca} ! / (n_O ! (n_{Ca} - n_O) !)$. Summarizing the above analyses, the normalized total number of ways of distribution is

$$\Omega = \frac{\left(\sum_{i=1}^4 in_{Q_i}/2 + n_{Ca}\right)!}{n_{Ca}! \left(\sum_{i=1}^4 in_{Q_i}/2\right)!} \times \frac{n_{Ca}!}{n_O!(n_{Ca} - n_O)!} \times \frac{(n_{Ca} - n_O)!}{\left(\prod_{i=0}^3 r_{ii}!\right) \prod_{i=0}^2 \prod_{j=i+1}^3 \left(\frac{r_{ij}! r_{ji}!}{2! 2!}\right)} \times \frac{\left(\sum_{i=1}^4 in_{Q_i}/2\right)!}{\left(\prod_{i=1}^4 b_{ii}!\right) \prod_{i=1}^3 \prod_{j=i+1}^4 \left(\frac{b_{ij}! b_{ji}!}{2! 2!}\right)} = \frac{\left(\sum_{i=1}^4 in_{Q_i}/2 + n_{Ca}\right)!}{n_O!} \times \left\{ \left(\prod_{i=0}^3 r_{ii}!\right) \prod_{i=0}^2 \prod_{j=i+1}^3 \left(\frac{r_{ij}! r_{ji}!}{2! 2!}\right) \right\}^{-1} \times \left\{ \left(\prod_{i=1}^4 b_{ii}!\right) \prod_{i=1}^3 \prod_{j=i+1}^4 \left(\frac{b_{ij}! b_{ji}!}{2! 2!}\right) \right\}^{-1} \quad (7)$$

With the application of the thermodynamic regulation that the configurational entropy should be the maximum when the system approaches equilibrium and the expression of the configurational entropy $S^{cf} = k \ln \Omega$ where k is the Boltzmann constant, Eq. (7) can be rewritten as

$$\Omega = \frac{\left(\sum_{i=1}^4 in_{Q_i}/2 + \sum_{i=0}^3 (4-i)n_{Q_i}/2 + n_O\right)!}{n_O!} \times \left\{ \prod_{i=0}^3 \frac{\left((4-i)n_{Q_i}\right)^2}{2 \sum_{i=0}^3 (4-i)n_{Q_i}} \right\} \times \prod_{i=0}^2 \prod_{j=i+1}^3 \left(\frac{(4-i)n_{Q_i} (4-j)n_{Q_j}}{2 \sum_{i=0}^3 (4-i)n_{Q_i}} \right) \times \left\{ \frac{(4-i)n_{Q_i} (4-j)n_{Q_j}}{2 \sum_{i=0}^3 (4-i)n_{Q_i}} \right\}^{-1} \times \left\{ \prod_{i=1}^4 \frac{\left(in_{Q_i}\right)^2}{2 \sum_{i=1}^4 in_{Q_i}} \right\} \times \prod_{i=1}^3 \prod_{j=i+1}^4 \left(\frac{in_{Q_i} jn_{Q_j}}{2 \sum_{i=1}^4 in_{Q_i}} \frac{in_{Q_i} jn_{Q_j}}{2 \sum_{i=1}^4 in_{Q_i}} \right) \right\}^{-1} \quad (8)$$

Expressing the configurational entropy with Eq. (8) and applying the Stirling formula $\ln m! \cong m \ln m - m$ when $m \rightarrow \infty$, we obtained

$$-\frac{S^{cf}}{k} = -\left(2 \sum_{i=0}^3 n_{Q_i} + n_O\right) \ln \left(2 \sum_{i=0}^3 n_{Q_i} + n_O\right) + n_O \ln n_O + \sum_{i=0}^3 \left(\frac{\left((4-i)n_{Q_i}\right)^2}{2 \sum_{i=0}^3 (4-i)n_{Q_i}} \ln \frac{\left((4-i)n_{Q_i}\right)^2}{2 \sum_{i=0}^3 (4-i)n_{Q_i}} \right) + 2 \sum_{\substack{i=0 \\ j=0 \\ i \neq j}}^3 \left(\frac{(4-i)n_{Q_i} (4-j)n_{Q_j}}{2 \sum_{i=0}^3 (4-i)n_{Q_i}} \ln \frac{(4-i)n_{Q_i} (4-j)n_{Q_j}}{2 \sum_{i=0}^3 (4-i)n_{Q_i}} \right) + \sum_{i=1}^4 \left(\frac{\left(in_{Q_i}\right)^2}{2 \sum_{i=1}^4 in_{Q_i}} \ln \frac{\left(in_{Q_i}\right)^2}{2 \sum_{i=1}^4 in_{Q_i}} \right) + 2 \sum_{\substack{i=1 \\ j=1 \\ i \neq j}}^4 \left(\frac{in_{Q_i} jn_{Q_j}}{2 \sum_{i=1}^4 in_{Q_i}} \ln \frac{in_{Q_i} jn_{Q_j}}{2 \sum_{i=1}^4 in_{Q_i}} \right) \quad (9)$$

Dividing the terms in above equation with $\sum_{i=0}^3 n_{Q_i} + n_{Ca} + n_O$ and representing the Boltzmann constant k with the molar gas constant R according to $R = N^0 \times k$ where N^0 is Avogadro constant, the final expression of configurational entropy can be achieved:

$$-\frac{S^{cf}}{R} = -\left(2 \sum_{i=0}^3 X_{Q_i} + X_O\right) \ln \left(2 \sum_{i=0}^3 X_{Q_i} + X_O\right) + X_O \ln X_O + \sum_{i=0}^3 \left(\frac{\left((4-i)X_{Q_i}\right)^2}{2 \sum_{i=0}^3 (4-i)X_{Q_i}} \ln \frac{\left((4-i)X_{Q_i}\right)^2}{2 \sum_{i=0}^3 (4-i)X_{Q_i}} \right) + 2 \sum_{\substack{i=0 \\ j=0 \\ i \neq j}}^3 \left(\frac{(4-i)X_{Q_i} (4-j)X_{Q_j}}{2 \sum_{i=0}^3 (4-i)X_{Q_i}} \ln \frac{(4-i)X_{Q_i} (4-j)X_{Q_j}}{2 \sum_{i=0}^3 (4-i)X_{Q_i}} \right) + \sum_{i=1}^4 \left(\frac{\left(iX_{Q_i}\right)^2}{2 \sum_{i=1}^4 iX_{Q_i}} \ln \frac{\left(iX_{Q_i}\right)^2}{2 \sum_{i=1}^4 iX_{Q_i}} \right) + 2 \sum_{\substack{i=1 \\ j=1 \\ i \neq j}}^4 \left(\frac{iX_{Q_i} jX_{Q_j}}{2 \sum_{i=1}^4 iX_{Q_i}} \ln \frac{iX_{Q_i} jX_{Q_j}}{2 \sum_{i=1}^4 iX_{Q_i}} \right) \quad (10)$$

With the combination of Eq. (5) and Eq. (10), we can calculate the thermodynamic properties from the microstructural information.

As mentioned somewhere above, the characteristic enthalpies and non-configurational entropies can be evaluated from two kinds of sources: the spectral and the

calorimetric. As the first application step of this model, the 10 parameters are still obtained from the calorimetric data of “corresponding single crystals” (Ca_2SiO_4 corresponding to Q_0 , $\text{Ca}_{1.5}\text{SiO}_{3.5}$ to Q_1 , CaSiO_3 to Q_2 , $\text{Ca}_{0.5}\text{SiO}_{2.5}$ to Q_3 and finally SiO_2 to Q_4). Here, the concept of “corresponding single crystal” (CSC) should be elucidated firstly. In 1975, BRAWER [28] suggested the concept of “corresponding crystal” to interpret the Raman spectra and structural units of silicate glasses. According to his definition, the structure of its unit cell is an average over all the structural units of glass. Mostly, those “corresponding crystals” are fictitious creation which may not exist in nature and whose existence may in fact be impossible. The idea of BRAWER was reformed by the present authors to define the concept of CSC, which corresponds to the minimum types of structural units in crystal with the same macro composition as the given melt. Practically, only the thermodynamic data for the real existing Ca_3SiO_5 , Ca_2SiO_4 , CaSiO_3 and SiO_2 can be found [13,29], but those for the unstable $\text{Ca}_{1.5}\text{SiO}_{3.5}$ and $\text{Ca}_{0.5}\text{SiO}_{2.5}$ lack. Fortunately, the relation of calorimetric properties of CSCs with the mole ratio of Ca to Si, just as shown in Fig. 1, is perfectly linear. Thus, the characteristic enthalpies and entropies of $\text{Ca}_{1.5}\text{SiO}_{3.5}$ and $\text{Ca}_{0.5}\text{SiO}_{2.5}$ can be reasonably and easily extrapolated from the experimental values of those stable CSCs.

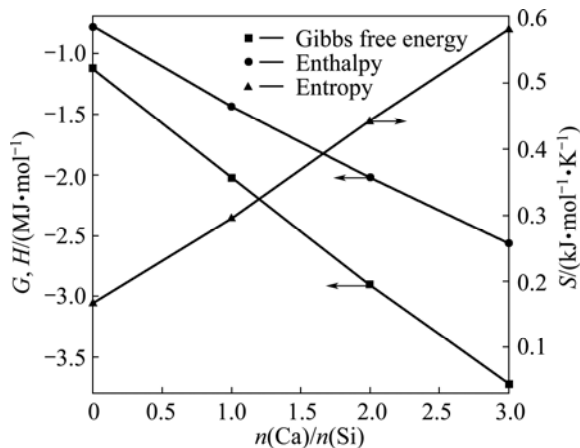


Fig. 1 Gibbs free energy, enthalpy and entropy of four real existed CSCs (It must be noted that molar thermodynamic quantities of G , H and S correspond to a mole of unit SiO_4 instead of a mole of $\text{CaO}+\text{SiO}_2$ although the quantities of $\text{Ca}_{1.5}\text{SiO}_{3.5}$ and $\text{Ca}_{0.5}\text{SiO}_{2.5}$ lack, they can be reasonably extrapolated from the data of the real existed CSCs)

It must be noted that the molar quantities of the G , H , and S in Fig. 1 correspond to a mole of unit SiO_4 instead of a mole of $\text{CaO}+\text{SiO}_2$. Here, S is not the non-configurational but the total entropy. In order to achieve the non-configurational entropy, the configurational part must be subtracted from the total.

Because only one or two kinds of Q_i s exist in any CSC under the constraint of minimum types of structural units, the molar fraction of Q_i can be directly calculated from the molar fraction of macro components. Thus, the configurational entropy can be directly calculated from Eq. (10) for all CSCs, just as shown in Fig. 2(a) and the result is displayed in Fig. 2(b). The vertical lines in Fig. 2(a) indicate the molar fractions of structural units of five CSCs with only one kind of Q_i and correspond to the minimum entropies highlighted by the five circles in Fig. 2(b). Subtracting the calculated configurational entropies of CSCs from the calorimetric entropies of five CSCs, the non-configurational entropies, or says, the characteristic entropies of Q_i s can be achieved. Then, the final values are collected in Table 4.

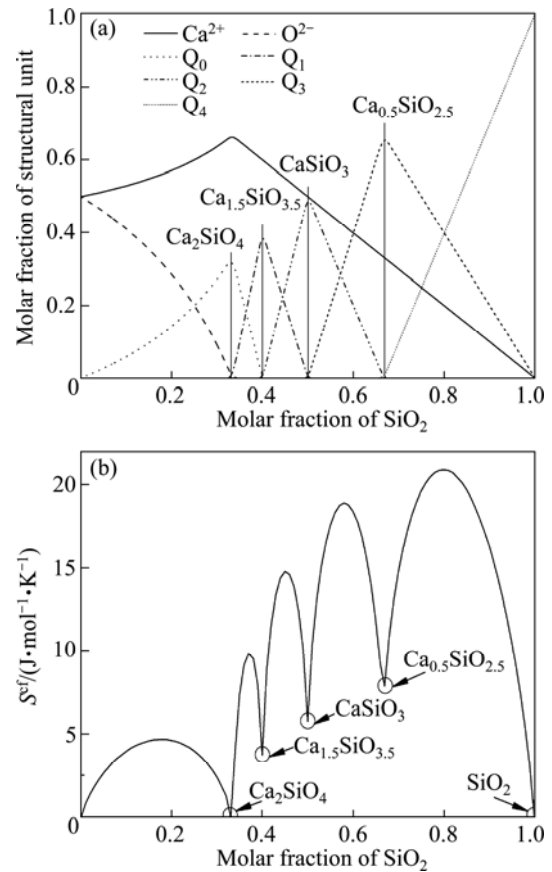


Fig. 2 Distribution of microstructural units (a) and corresponded configurational entropy (b) of CSCs for full composition range

Above deduction of this model implies its future utilization as the subsequent application of some structural analyzing experiments, such as Raman and NMR spectra. But the first step is to make this model self-consistent using the optimization mechanism to find the minimum of Gibbs free energy under a certain thermodynamic condition. At the same time, the relative abundance of structural units corresponding to the minimum of systematic Gibbs free energy is also

Table 4 Characteristic enthalpies and entropies at 2000 K for calcium silicate melts

Melt	$H_{Q_{i,0}} /$ (kJ·mol ⁻¹)	$S_{Q_{i,0}} /$ (kJ·mol ⁻¹ ·K ⁻¹)	$S_{Q_{i,0}}^{cf} /$ (kJ·mol ⁻¹ ·K ⁻¹)	$S_{Q_{i,0}}^{ncf} /$ (kJ·mol ⁻¹ ·K ⁻¹)
Ca ₂ SiO ₄ (Q ₀)	-2000.71	0.4405	0	0.4405
Ca _{1.5} SiO _{3.5} (Q ₁)	-1704.79	0.3713	0.0094	0.3620
CaSiO ₃ (Q ₂)	-1408.86	0.3022	0.0115	0.2907
Ca _{0.5} SiO _{2.5} (Q ₃)	-1112.94	0.2331	0.0118	0.2213
SiO ₂ (Q ₄)	-817.01	0.1639	0	0.1639

automatically obtained, which is why we call the model self-consistent. From optimization theory, this optimizing process can be treated as the optimization problem under linear restrictions and resolved with the method of penalty function [30]. The express of the optimization of Gibbs free energy is

$$\begin{aligned} \min G(\mathbf{X}) \\ \text{s.t. } \mathbf{AX} \geq \mathbf{b} \\ \mathbf{CX} = \mathbf{d} \end{aligned} \quad (11)$$

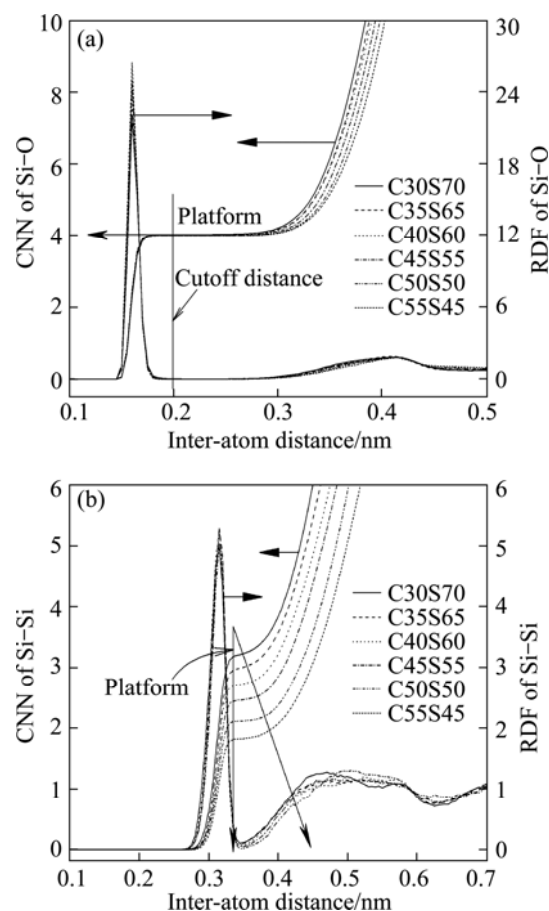
where s.t. means satisfactory restrictions. The terms in above equation are all extended and interpreted in appendix.

3 Results and discussion

3.1 Static and statistic structural properties from MD simulation

Partial radial distribution functions (RDFs) and corresponding coordinate number functions (CNNs) of Si–O and Si–Si, which are most important for the understanding of the distribution of structural units, are presented in Fig. 3.

In these simulations, the average pair distances of Si–O, Ca–O, O–O and Si–Si are within the ranges of 1.613–1.617 Å, 2.350–2.356 Å, 2.624–2.626 Å and 3.170–3.194 Å for all six samples. WASEDA and TOGURI [31] determined the four quantities of CaSiO₃ melt by X-ray diffraction, orderly 1.61 Å, 2.35 Å, 2.67 Å and 3.21 Å, and the following three quantities of SiO₂, 1.62 Å, 2.65 Å and 3.12 Å. BELASHCHENKO et al [5] simulated the structures of alkaline earth silicate melts and obtained the quantities of 1.63 Å, 2.31 Å, 2.65 Å and 3.26 Å for molten calcium silicate. KEEN and DOVE [32] quantified the relationship between the atomic structures of the amorphous, the ordered and disordered crystalline phases of silica using neutron total scattering measurements, and gave the quantities of Si–O, O–O and Si–Si for α -quartz, 1.609 Å, 2.616–2.645 Å and

**Fig. 3** RDFs and CNNs of Si–O and Si–Si from MD simulation

3.059 Å. All of these quantities, from not only calculations but also XRD and neutron scattering, are in agreement with each other very well. Additionally, both CNNs in Fig. 3 of Si–O and Si–Si have platforms. The CNN platform of Si–O indicates the stable structural units via the corresponding y-axis value, whereas that of Si–Si reveals the connection between the units. From Fig. 3, a traditional conclusion can be achieved that the Si–O tetrahedron, which corresponds to the y-axis value of platform, i.e. 4, mainly constructs the network structure. Meanwhile, the platform of Si–Si, which can also offer the average coordinate number and consequently the degree of the systematic polymerization, becomes broader and lower with the decrease of SiO₂. Pickup of the y-axis values of Si–Si platforms demonstrates a linear correlation with the molar fraction of CaO, as shown in Fig. 4. The rate of the line slope is -0.05667 . If Ca is complete network modifier and Si is network former, the ideal rate should be -0.06 , which is slightly lower than the simulated value. Thus, we can say that Ca plays a very strong network modifier role in the structure of silicate melt.

According to the sorting of bridging and non-bridging oxygen, Si–O can also be divided into Si–O_b and Si–O_{nb}, where O_b and O_{nb} denote the bridging

and non-bridging oxygen. The average bond lengths of Si–O_b and Si–O_{nb}, which is very important for the vibrational properties, are displayed in Fig. 5. It is obvious that the effect of composition on Si–O_{nb} length is much stronger than that on Si–O_b. This character can explain the frequency-shifting phenomenon in the experimental Raman spectra.

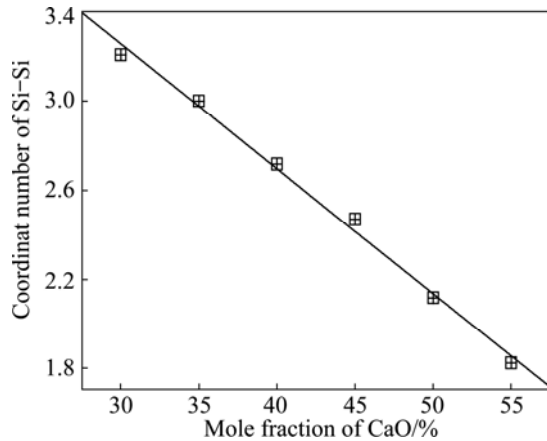


Fig. 4 Average coordinate number of Si-Si extracted from CNNs of Si-Si

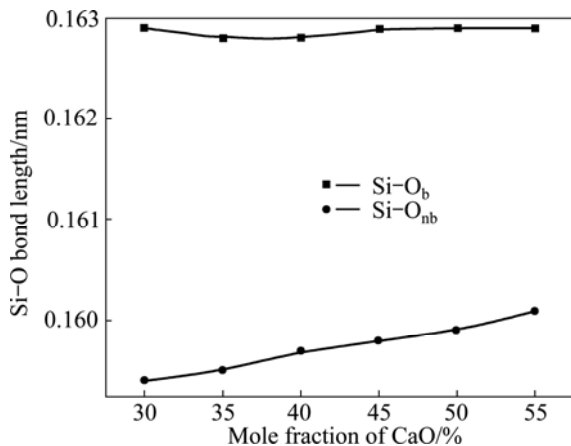


Fig. 5 Bond lengths of Si–O_b and Si–O_{nb} from MD simulation

For the main purpose, the simulated equilibrium configurations are decomposed into five kinds of Si–O tetrahedral units and the concentrations are listed in Table 5. In the decomposition process, two steps were performed: the first is to search for the coordinated oxygen in the whole configuration including the images in the neighboring periodic boxes, and the next is to determine the number of bridging oxygen in each tetrahedron, which includes the judgment of bridging or non-bridging oxygen. That's to say, a cutoff distance must be provided in order to determine whether the selected Si–O pair is bonded with each other. From Fig. 3(a), a reasonable cutoff distance, 0.2 nm, can be achieved. In fact, any value falling into the range of about 0.19–0.26 nm, which corresponds to the first

minimum of pair RDF of Si–O, can be selected as the cutoff distance. By comparing with the NMR results of the alkaline silicate glasses [33], the simulated distribution of calcium silicate melts is broader but has a very similar trend. These simulated concentrations will be discussed by comparing with the results of experimental Raman spectra and our thermodynamic model later.

Table 5 Simulated concentrations of Si–O tetrahedral units (molar fraction)

Sample	Q ₀	Q ₁	Q ₂	Q ₃	Q ₄
C30S70	0	0.0191	0.1509	0.4385	0.3915
C35S65	0	0.0408	0.2219	0.4471	0.2902
C40S60	0	0.0583	0.2891	0.4374	0.2010
C45S55	0	0.1181	0.3593	0.4230	0.0996
C50S50	0.0430	0.1763	0.3955	0.3346	0.0506
C55S45	0.0618	0.2663	0.4146	0.2387	0.0186

3.2 Results of structural thermodynamic model and comparison of three kinds of results

One can tell that the results from both MD simulations and experiments are discrete but not continuous. Therefore, the structural thermodynamic model was constructed to give the panorama of the distribution of Q_i. Figure 6(a) displays the complete distribution at 2000 K when the normalization condition is acted on the whole microstructural units,

$$\sum_{i=0}^4 X_{Q_i} + X_{Ca} + X_O = 1.$$

We can find that the free oxygen appears only in the region of $X_{SiO_2} < 0.33$, which has been proven by various experimental and theoretical studies. Because most researchers in this and related fields are more concerned about the distribution of five Q_s in the composition range of $0.33 < X_{SiO_2} < 1$ when $X_{Q_0} + X_{Q_1} + X_{Q_2} + X_{Q_3} + X_{Q_4} = 1$, Fig. 6(b) also shows this kind of distribution. In 1991, MAEKAWA et al [33] have studied the distribution of Q_s in alkaline silicate glasses instead of melts by means of ²⁹Si NMR and the changing trend with the composition is very similar with the results of our model. Meanwhile, the distributions of Q_s from MD simulation and thermodynamic model have been compared with each other in Fig. 6(c) in addition to experimental data from Raman spectra [11,22,34], and give a very good agreement, especially the results of MD simulation and thermodynamic model.

The original spectra [11, 22, 34] show a very clear effect of temperature and frequency on the intensity and the background radiation makes it very difficult to compare with each other. Thus, the corrected lines for temperature- and frequency-dependent scattering intensity [35] are used. All spectral lines have two

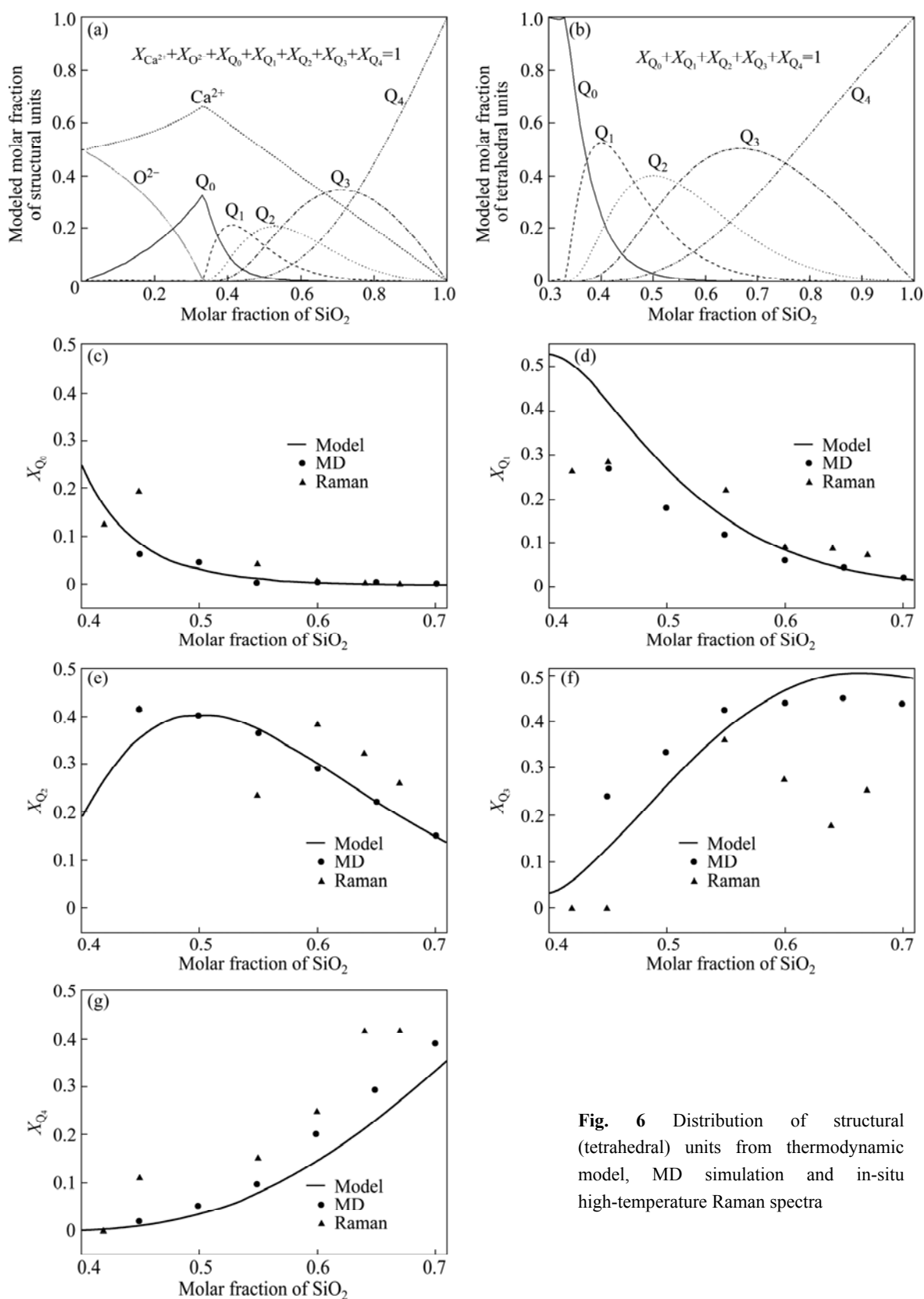


Fig. 6 Distribution of structural (tetrahedral) units from thermodynamic model, MD simulation and in-situ high-temperature Raman spectra

envelopes located at 500–700 cm⁻¹ and 600–1200 cm⁻¹, respectively. Meanwhile, the series of envelopes change systematically with the calcium oxide concentration. With the increase of calcium oxide, the frequency of

high-frequency envelope shifts from about 1030 to 860 cm⁻¹ and that of medium-frequency envelope shifts from 550 to 620 cm⁻¹. The similar phenomenon occurs for the intensities of these two envelopes. According to our

previous theoretical study of Raman spectra [22,36], the medium-frequency envelope is mainly contributed by the symmetrical bending of bridging oxygen (SBB mode) Si–O_b–Si, and for the high-frequency envelope, the symmetrical stretching (SS mode) of the Si–O bonds in tetrahedron and further analysis indicate that the contribution of stretching motion of non-bridging oxygen to SS mode is much greater than that of bridging oxygen. From the MD simulated results in Fig. 5, the bond length of Si–O_{nb} becomes longer with the increase of CaO, but very slight change for Si–O_b. That's to say, with the increase of CaO, the action of Si on O_{nb} becomes weaker and consequently the red shift of high-frequency envelope occurs with the change of composition. Plenty of works have proved that the high-frequency envelope in Raman spectra is contributed by various Q_i except Q₄. Thus, in order to achieve the concentration of Q_i, the high-frequency envelopes should be deconvolved into several single bands just overlapped with each other as follows: 810–850 cm⁻¹ for Q₀, 900–950 cm⁻¹ for Q₁, 1000–1050 cm⁻¹ for Q₂ and ~1100 cm⁻¹ for Q₃, from the reviews of McMILLAN [12] and the studies of BRAWER and WHITE [37] about the Raman shifts of silicate glasses and crystals. As for the SS mode of Q₄ in the high-frequency region, its intensity is so weak that no signal for it can be detected even in the spectra of amorphous SiO₂. The theoretical explanation for the frequency and intensity regulations can be found in Refs. [22,36]. From the Raman scattering theory, the area fractions under the characteristic bands do not directly represent their relative abundance. There is a factor named Raman scattering coefficient defined as follows:

$$A_i = M_i \times C_i \quad (12)$$

where M_i , A_i and C_i denote the molar fraction, area fraction of characteristic band of Q_i and its corresponding Raman scattering coefficient, respectively. A major difficulty in computing the relative abundances of Q_is from Raman spectra lies in the determination of these relative Raman scattering coefficients. In studies of alkali silicate melts, MYSEN and FRANTZ [17] used NMR data [38] in conjunction with their Raman data for sodium silicate to calculate the ratio of Raman scattering coefficients for Q₃ and Q₂. YOU et al [34] have also given the same ratio with the inner standard of polycrystal NaNO₂ powder. In this work, we used our theoretical results of the five relative C_i [36,39]: 1.0 for Q₀, 0.518 for Q₁, 0.249 for Q₂, 0.099 for Q₃ and 0.016 for Q₄, which agree very well with the experimental values of MYSEN and FRANTZ [17] and YOU et al [34]. By dividing the coefficients from A_i as shown in Eq. (12), we can obtain the relative abundance of Q₀–Q₃. To further achieve the abundance of Q₄, the mass conservation formulated by Eq. (3) must be used. Then, after the normalization process we obtained the final

molar fractions of Q_i from Raman spectra as shown in Fig. 6.

The theories applied in these three kinds of methods are completely different from each other, but they achieved agreeable results. The key is the equilibrium of system. Although the Raman spectra root in the vibrations of structural units, but the system when being measured are in a macro-thermodynamic equilibrium condition, which indicates that the Gibbs free energy of system is the minimum and this condition is just the only convergence condition of the thermodynamic model. As for the MD simulation, when analyzing the distribution of units, the simulated system has been relaxed around the equilibrium state for a period of time. So, all the three methods gave a unique distribution of units under thermodynamic equilibrium and that's to say, reached the same goal by different routes. The initial purpose to construct this thermodynamic model is to calculate the equilibrium thermodynamic properties of silicate melts with the utilization of the microstructural information obtained from spectral measurements, e.g. high-temperature Raman spectra and NMR. So, the agreement has partly proven the probability of this kind of application. Attention should be paid to a fact that this model can only be applied to the melts instead of glasses because the glasses are in the unstable state, which is not met for the basic demand of this model.

From the viewpoint of structural thermodynamics, the master of the distribution of Q_i in equilibrium is so-called disproportionating reactions between different Q_is:

$$2Q_i = Q_{i-1} + Q_{i+1} \quad (13)$$

Farther analysis of Fig. 6(b) can achieve the following five divisions in the composition range of 0.33 < X_{SiO₂} < 1, which indicates the different mastering reactions in different divisions just as listed in Table 6. With the instruction of Table 6, the further studies of determination of the equilibrium constants of these three kinds of disproportionating reactions become possible.

Table 6 Mastering disproportionating reactions in different divisions corresponding to five divisions

Division (molar fraction of SiO ₂)	Mastering disproportionating reaction
0.33–0.36	2Q ₁ =Q ₀ +Q ₂
0.36–0.41	2Q ₁ =Q ₀ +Q ₂ , 2Q ₂ =Q ₁ +Q ₃
0.41–0.66	2Q ₁ =Q ₀ +Q ₂ , 2Q ₂ =Q ₁ +Q ₃ , 2Q ₃ =Q ₂ +Q ₄
0.66–0.76	2Q ₂ =Q ₁ +Q ₃ , 2Q ₃ =Q ₂ +Q ₄
0.76–1.00	2Q ₃ =Q ₂ +Q ₄

3.3 Distribution of connections of Q_i -Ca- Q_j and Q_i -[O_b]- Q_j

Between the tetrahedral units, two kinds of connections are introduced denoted as Q_i -Ca- Q_j and Q_i -[O_b]- Q_j , which represent, the connection via the electrovalent bond between non-bridging oxygen O_{nb} and cation Ca²⁺ and the connection via sharing bridging oxygen O_b, respectively. In fact, these connections indicate the properties of super structural units in calcium silicate melt, such as the rings, sheets, chains and disordered three-dimension network. They are also the important structural properties to influence the macro thermodynamic and dynamic properties.

In our thermodynamic model, after the achievement of distribution of Q_i , we can estimate the distributions of these two kinds of connections. Because the configurational entropy is the direct quantification of these distributions, and so, we can obtain the following relations according to the equilibrium condition:

$$R_{ij} \propto (4-i)X_{Q_i}(4-j)X_{Q_j} \quad (14)$$

$$B_{ij} \propto iX_{Q_i}jX_{Q_j} \quad (15)$$

where R_{ij} represents the fraction of connection of Q_i -Ca- Q_j and B_{ij} is the fraction of Q_i -[O_b]- Q_j . Above relations are just proportional and consequently, the calculated quantities of R_{ij} and B_{ij} must be normalized obeying the normalization restrictions of

$$\sum_{\substack{i=0 \\ j \geq i}}^3 R_{ij} = 1 \quad \text{and} \quad \sum_{\substack{i=1 \\ j \geq i}}^4 B_{ij} = 1.$$

The results are displayed in Fig. 7. In the past century, most attentions were paid to the so-called equivalent connections, especially the equivalent connection between the same Q_i via bridging oxygen, e.g. Q_4 -[O_b]- Q_4 , Q_3 -[O_b]- Q_3 etc. For example, most studies, e.g. Ref. [40], of the vibrational spectra of complex structural units of amorphous silicates were always concentrated to the ring, chain or sheet constructed with same kind of Q_i s, which indicate that all the connections in the structural cells are equivalent. These are based on an assumption that in silicate melt, equivalent connection always precedes non-equivalent connection. This assumption has never been verified but is supported for the first time by our calculation of the distribution of connections to some extent. As shown in Fig. 7, the bold lines, which figure the distribution of dominant connections, are all constructed with the equivalent connections. That's to say, for any composition, the most dominant connection is equivalent connections. Additionally, with the reference of the distribution of Q_i (Fig. 6(b)), it can be found that the compositions corresponding to the maximum of equivalent connection

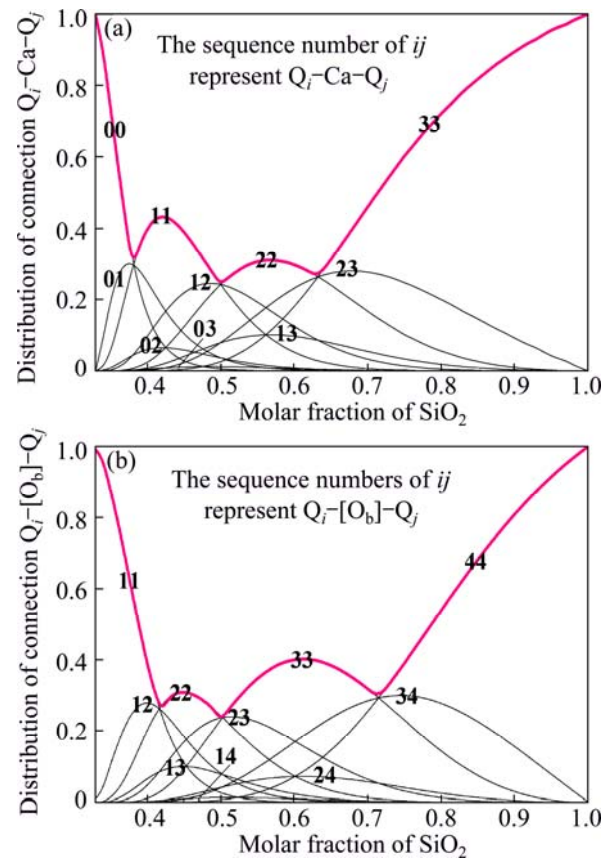


Fig. 7 Distributions of connection of Q_i -Ca- Q_j (a) and Q_i -[O_b]- Q_j (b) (The bold lines figure the distribution of dominant connections)

are different from the compositions corresponding to the maximum of the tetrahedral units: the location of maximum of Q_i -Ca- Q_i shifts to the right side relative to the position of the maximum of Q_i and that for Q_i -[O_b]- Q_i shifts to the left, e.g. $X_{\text{SiO}_2}(R_{22}^{\text{max}}) > X_{\text{SiO}_2}(X_{Q_2}^{\text{max}}) > X_{\text{SiO}_2}(B_{22}^{\text{max}})$.

4 Conclusions

In this work, two methods were applied to studying the distribution of microstructural units in CaO-SiO₂ melts. Firstly, MD simulation gave the result that the average coordinate number of oxygen around silicon is very stable, 4, which indicates that the stable structural units in calcium silicate melts are different Si-O tetrahedra. Secondly, we present the deduction of a newly constructed thermodynamic model from the basic definition of microstructural units. Finally, by comparing the discrete results from MD simulation and referenced Raman spectra with the continuous result of the newly constructed thermodynamic model, we reached the same goal by different routes and obtained the panorama distribution of Q_i and their connections.

- [21] JIANG G C, YOU J L, YU B K, HAUNG S P. Developments of high temperature Raman spectroscopic techniques [J]. Spectroscopy and Spectral Analysis, 2000, 20(2): 206–209.
- [22] WU Y Q, JIANG G C, YOU J L, HOU H Y, CHEN H, XU K D. Theoretical study of the local structure and Raman spectra of CaO–SiO₂ binary melts [J]. Journal of Chemical Physics, 2004, 121(16): 7883–7895.
- [23] MATSUMIYA T, NOGAMI A, FUKUDA Y. Applicability of molecular dynamics to analyses of refining slags [J]. ISIJ International, 1993, 33(1): 210–217.
- [24] KIEFFER J, ANGELL C A. Structural incompatibilities and liquid–liquid phase separation in molten binary silicates: A computer simulation [J]. The Journal of Chemical Physics, 1989, 90(9): 4982–4991.
- [25] HOOVER W G. Canonical dynamics: Equilibrium phase-space distributions [J]. Physical Review A, 1985, 31(3): 1695–1697.
- [26] REFSON K. Moldy user's manual [M]. Revision 2.26. Oxford: Department of Earth Sciences, 2001.
- [27] ALLEN M P, TILDESLEY D J. Computer simulation of liquids [M]. Oxford: Clarendon Press, 1987.
- [28] BRAWER S. Theory of the vibrational spectra of some network and molecular glasses [J]. Physical Review B, 1975, 11(8): 3173–3194.
- [29] PELTON A, BLANDER M. Thermodynamic analysis of ordered liquid solutions by a modified quasichemical approach—Application to silicate slags [J]. Metallurgical Transactions B, 1986, 17(4): 805–815.
- [30] XUE Jia-qing. Theory and methods of optimization [M]. Beijing: Press of Metallurgical Industry, 1995. (in Chinese)
- [31] WASEDA Y, TOGURI J M. The structure of molten binary silicate systems CaO–SiO₂ and MgO–SiO₂ [J]. Metallurgical Transactions B, 1977, 8(3): 563–568.
- [32] KEEN D A, DOVE M T. Local structures of amorphous and crystalline phases of silica, SiO₂, by neutron total scattering [J]. Journal of Physics: Condensed Matter, 1999, 11: 9263–9273.
- [33] MAEKAWA H, MAEKAWA T, KAWAMURA K, YOKOKAWA T. The structural groups of alkali silicate glasses determined from ²⁹Si MAS-NMR [J]. Journal of Non-Crystalline Solids, 1991, 127(1): 53–64.
- [34] YOU J L, JIANG G C, XU K D. High temperature Raman spectra of sodium disilicate crystal, glass and its liquid [J]. Journal of Non-Crystalline Solids, 2001, 282(1): 125–131.
- [35] LONG D A. Raman spectroscopy [M]. New York: McGraw-Hill, 1977.
- [36] WU Y Q, JIANG G C, YOU J L, HOU H Y, CHEN H. Raman scattering coefficients of symmetrical stretching modes of microstructural units in sodium silicate melts [J]. Acta Physica Sinica, 2005, 54(2): 961–966.
- [37] BRAWER S A, WHITE W B. Raman spectroscopic investigation of the structure of silicate glasses. I. The binary alkali silicates [J]. The Journal of Chemical Physics, 1975, 63(6): 2421–2432.
- [38] STEBBINS J F. Effects of temperature and composition on silicate glass structure and dynamics: Si-29 NMR results [J]. Journal of Non-Crystalline Solids, 1988, 106(1–3): 359–369.
- [39] WU Y Q, YOU J L, JIANG G C, CHEN H. Theoretical study of structural and Raman spectral properties of CaSiO₃ quenched from melt to glass [J]. Chinese Journal of Inorganic Chemistry, 2004, 20(2): 133–138. (in China)
- [40] SITARZ M, MOZGAWA W, HANDKE M. Vibrational spectra of complex ring silicate anions—Method of recognition [J]. Journal of Molecular Structure, 1997, 404(1–3): 193–197.

硅酸钙熔体局域结构的经典分子动力学模拟与结构热力学模型比较

吴永全, 戴辰, 蒋国昌

上海大学 材料科学与工程学院, 现代冶金与材料制备重点实验室, 上海 200072

摘要: 通过经典分子动力学模拟及一个新建的结构热力学模型计算获得了硅酸钙熔体的局域结构单元的全程分布。将这两种方法获得的 5 种 SiO 四面体的 Q_i 分布进行比较, 并与 Raman 光谱实验结果进行比较, 结果吻合得非常好。这不仅给出了微结构单元在全成分范围内的全景分布, 而且证明了我们的模型适合于针对光谱实验数据的后续热力学计算。与此同时, 由不同歧化反应控制的 5 个成分区间也被精确划分。还从该结构热力学模型中首次获得了 Q_i 之间的两种连接方式 Q_i -Ca- Q_j 和 Q_i -[O_b]- Q_j 的分布情况, 并由此证明所有成分中都是以等价连接为主要的连接方式。

关键词: 微观结构单元分布; 分子动力学模拟; 结构热力学模型; 硅酸钙熔体

(Edited by Hua YANG)